Journal of
BIOPHOTONICS

FULL ARTICLE

Monitoring implantable immunoisolation devices with intrinsic fluorescence of genipin

Edorta Santos-Vizcaino[1,2] | Henry Haley[3] | Ainhoa Gonzalez-Pujana[1,2] | Gorka Orive[1,2] |
Rosa Maria Hernandez[1,2] | Gary D. Luker[3,4,5]* | Jose Luis Pedraz[1,2]*

[1]NanoBioCel Group, Laboratory of Pharmaceutics, School of Pharmacy, University of the Basque Country (UPV/EHU), Vitoria-Gasteiz, Spain

[2]Biomedical Research Networking Centre in Bioengineering, Biomaterials and Nanomedicine (CIBER-BBN), Vitoria-Gasteiz, Spain

[3]Department of Radiology, Center for Molecular Imaging, University of Michigan Medical School, Ann Arbor, Michigan

[4]Department of Biomedical Engineering, University of Michigan Medical School, Ann Arbor, Michigan

[5]Department of Microbiology and Immunology, University of Michigan Medical School, Ann Arbor, Michigan

*Correspondence
Jose Luis Pedraz, NanoBioCel Group, Laboratory of Pharmaceutics, School of Pharmacy, University of the Basque Country (UPV/EHU), Vitoria-Gasteiz 01006, Spain.
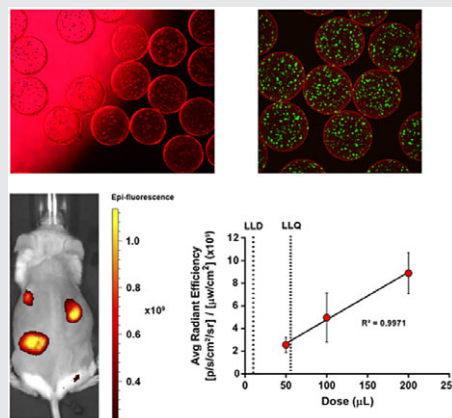Email: joseluis.pedraz@ehu.eus
Gary D. Luker, Department of Radiology, Center for Molecular Imaging, University of Michigan Medical School, Ann Arbor, MI 48109.
Email: gluker@med.umich.edu

Imaging of implanted hydrogel-based biosystems usually requires indirect labeling of the vehicle or cargo, adding complexity and potential risk of altering functionality. Here, for the first time, it is reported that incorporation of genipin into the design of immunoisolation devices can be harnessed for in vivo imaging. Using cell-compatible in situ cross-linking reactions, a fast, efficient and noncytotoxic procedure is shown to maximize fluorescence of microcapsules. Moreover, genipin is validated as a quantitative imaging probe by injecting increasing doses of microcapsules in the subcutaneous space of mice, obtaining strong, stable fluorescence with good linearity of signal to microcapsule dose over several weeks. This allows immediate assessment of the actual injected dose and monitoring of its position over time, thereby significantly enhancing the efficacy and biosafety of the therapy. These outcomes may facilitate clinical translation and optimize medical applications of multiple hydrogel-based biotechnologies.

KEYWORDS

biosafety, genipin, hydrogels, immunoisolation devices, quantitative imaging

1 | INTRODUCTION

Designing hydrogel technologies for detection by imaging frequently requires modifying the hydrogel itself [1, 2] or the cargo [3], adding complexity to overall design and potentially altering mechanical and functional characteristics [4]. We sought to overcome these challenges by incorporating a biomaterial with inherent imaging properties into device design. While applicable broadly to other areas in biotechnology, in the present study we focus on immunoisolation devices consisting of alginate microspheres coated with a semipermeable membrane formed by polycations (usually poly-L-Lysine or poly-L-ornithine). The membrane protects the encapsulated cell content against immune cell and antibody mediated host's rejection, while allowing the inward diffusion of nutrients and oxygen, and the release of bioactive compounds into the surrounding tissue. This approach currently is one of the leading strategies to deliver bioactive molecules from immobilized allo- or xenogenic cells [5, 6]. To date, remarkable outcomes have been obtained in clinical

trials for the treatment of chronic diseases such as diabetes [7, 8] or cancer [9, 10]. However, development of a suitable noninvasive visualization strategy that provides relevant information about implanted microcapsules becomes crucial to make the definitive leap to the clinic [11–13].

In this sense, one of the main problems lies in the impossibility to ensure the correct administration of the intended dose. This is because, to the best of our knowledge, to date there is no tool to immediately assess (quantitatively) the actual injected dose and then monitor its position and stability for long periods of time (maintaining a reliable, precise and stable signal/dose relation). Alternative imaging strategies, such as reporter genes based on luciferase or fluorescence proteins, provide poor information immediately after injection, since the hypoxic stress suffered by encapsulated cells during the first days postimplantation makes the emitted signal unreliable [14–16].

Genipin is a natural compound with dual properties that uniquely meet the demand for a hydrogel technology detectable through imaging. Strikingly, while benefits of genipin as a cross-linker are increasingly appreciated due to its superior biocompatibility, use of natural fluorescence from this material has generally been overlooked or considered only anecdotally [17–20]. Contrarily, in the nano-scale, genipin-cross-linked globin-PEI nanoparticles [21] and genipin cross-linked ovalbumin protein nanoparticles [22] have been recently reported as suitable for in vivo imaging. However, described methods are far from being applicable to higher scaled cell-laden hydrogels for cell therapies. Indeed, to the best of our knowledge, no one has achieved a cytocompatible in situ cross-linking of genipin with optimal brightness for in vivo imaging of hydrogel technologies.

Here, for the first time, we harness the natural fluorescence of genipin to produce bright, quantitative and stable fluorescence for in vivo imaging of cell-laden hydrogel systems. Following excitation with red light, genipin emits far-red fluorescence with a broad tail extending into the near infra-red spectrum (Figure S1 in Appendix S1, Supporting Information) [21]. These wavelengths of light are highly favorable for in vivo imaging studies, particularly for hydrogels designed for implantation in superficial sites such as subcutaneous, subdermal, or intraocular [23]. Our results obtained with alginate-poly-L-Lysine immunoisolation devices show that fluorescence from genipin meets the need for quantitative imaging of implanted biomaterials. By incorporating a biomaterial with inherent imaging properties into device design, this ground-breaking advance will facilitate clinical translation of a wide range of hydrogel technologies for cell-based therapies and tissue engineering.

2 | RESULTS AND DISCUSSION

To obtain a good signal to noise ratio for imaging in vivo, maximizing the fluorescence becomes indispensable. Thus,

we first optimized the cross-linking procedure of genipin while maintaining cell viability using D1 mesenchymal stem cells from Balb/c mice genetically engineered to secrete human erythropoietin (D1-MSC-hEPO). We subjected cells encapsulated in alginate-poly-L-Lysine (AP) to different combinations of genipin concentrations (0.001%, 0.01% and 0.1%) and exposure times (5, 15, 30 and 60 minutes at room temperature) (Figure 1A). For each grouping, we recorded fluorescence intensity of the microspheres (Ex: 590 nm; Em: 630 nm) and viability of encapsulated cells. We plotted results as a function of these two variables (Figure 1B,C). As a control group, we used cells immobilized in noncross-linked AP microcapsules. Based on these screening assays, we chose the best four conditions where we obtained the highest fluorescence intensities with statistically nonsignificant losses in viability compared with the AP control group (Figure 1B,C, white points): 0.01% and 30 minutes < 0.01% and 60 minutes < 0.1% and 5 minutes < 0.1% and 15 minutes ($P < 0.001$ for all comparisons) (Figure S2 in Appendix S1).

After examining these four protocols in detail (Figure 1D), we chose 0.1% genipin and 5 minutes exposure time as the optimum conditions. Despite rendering lower fluorescence intensity than the 0.1% and 15 minutes combination, the latter showed more internal fluorescence (cross-linked cells), so we preferred shorter exposure times to accelerate the coating process and allow greater flexibility and safety margin with respect to cell viability. Indeed, most studies to date use longer exposure times to genipin (from 30 minutes to 24 hours) [17, 20, 24], which may limit dramatically the applicability of this cross-linking agent for cell microencapsulation purposes. Thus, our genipin-meditated cross-linking procedure is fast, efficient and noncytotoxic, even in the presence of cells.

With the aim of maximizing fluorescence signal of the microcapsules, we next added a second coating of poly-L-Lysine (PLL) cross-linked with genipin, following the same protocol described above (0.1% genipin and 5 minutes exposure). This process produced genipin-cross-linked double poly-L-Lysine membranes (GDP) (see 3D morphology in Video S1, Supporting Information). As intermediate control groups, we also tested AP microcapsules cross-linked with genipin (APG), AP with a second PLL coating (APP) and APG microcapsules with an additional covering of PLL (APGP) (Figure 2A). All genipin-containing groups developed maximum fluorescence values after 72 to 96 hours periods of incubation (cell culture conditions, after exposure to genipin) (Figure 2B), following a first-order reaction (Figure S3 in Appendix S1). Interestingly, we could clearly observe that GDP microcapsules emitted 6-fold higher fluorescence intensity than APG and APGP counterparts ($P < 0.01$ and 0.001, respectively) (Figure 2C,D), probably due to increased availability of PLL for cross-linking. This gain in fluorescence is essential for maximizing the signal to
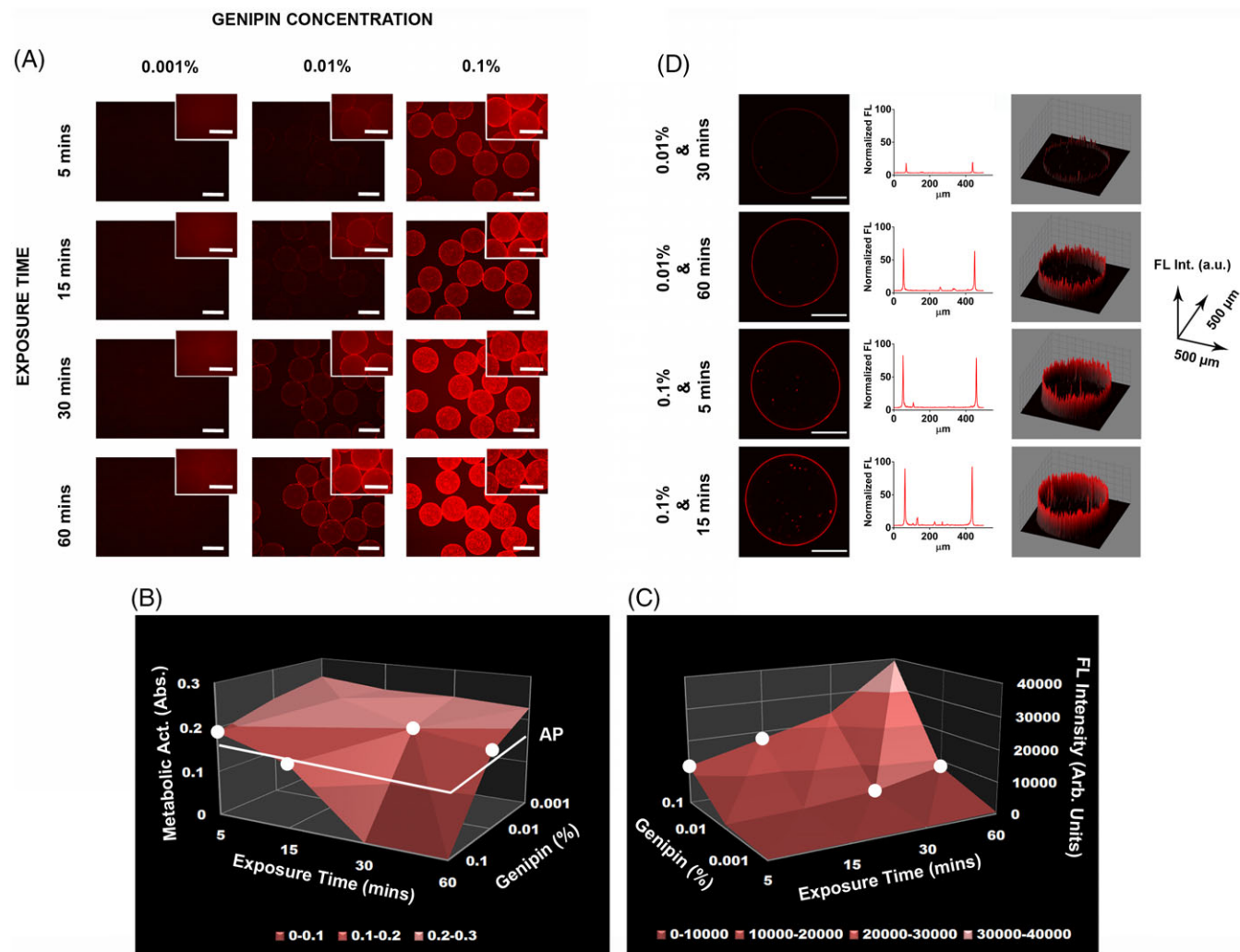
FIGURE 1 Optimization of genipin cross-linking procedure in cell-laden microcapsules. D1-MSC-hEPO cells enclosed within AP microcapsules were subjected to increasing genipin concentrations (0.001%, 0.01% and 0.1%) and exposure times (5, 15, 30 and 60 minutes) to find the optimum conditions. A, Representative epi-fluorescence micrographs of each concentration and time combination. Scale-bar, 400 μm. B, Three-dimensional plot representing mean metabolic activity values of encapsulated cells in function of different genipin concentrations and exposure times. The white line indicates the mean value from noncross-linked AP control group. C, Three-dimensional plot representing mean fluorescence intensities of AP microcapsules in function of different genipin concentrations and exposure times. B, C, Color scale from light red to dark red denotes highest and lowest values, respectively. The white points depict the highest fluorescence signal intensities obtained without affecting cell viability (nonsignificant differences against cells encapsulated in noncross-linked AP microcapsules, $P > 0.05$). Statistical analysis: one-way ANOVA with Bonferroni multiple comparison correction, $n = 5$ samples for each assay. D, Analysis of the conditions selected in (B, C) by means of confocal fluorescence microscopy. From left to right: representative confocal fluorescence micrographs, profile lines and 3D surface plots of the fluorescence signal distribution and intensity from the equatorial section of microcapsules. Scale bar, 200 μm. FL, fluorescence

noise ratio for imaging in vivo. In addition, we easily can augment fluorescence intensity by producing smaller size microcapsules. Here, we obtained a 2.5-fold-increase in fluorescence intensity by just reducing diameter of microcapsules by 33% ($P < 0.01$) (Figure S4 in Appendix S1).

To exclude any negative effects on cell integrity and function as a consequence of incorporating so many variations in microcapsule design, we tested different control groups to detect possible problems at any step of the formulation. The protocol for producing GDP microcapsules reliably maintained viability of encapsulated cells (Figure 2E,F and Video S2) and the capacity of immobilized cells to secrete high rates of therapeutic product, in this case human

erythropoietin (hEPO) (Figure 2G). All these assays showed no significant differences with respect to the AP control group.

Then, we tested performance of GDP microcapsules as a monitoring system for in vivo imaging. For such aim, we implanted 50, 100 or 200 μL of GDP microcapsules (Figure 3A) into the subcutaneous space of NSG mice. Images obtained with 570 nm excitation and a 620/20 emission filter exhibited a strong signal with excellent signal to noise ratio for all injections (Figure 3B). Importantly, we also achieved a good linearity of fluorescence response to microcapsule dose ($R^2 = 0.9971$) (Figure 3C). We next monitored fluorescence of genipin at days 1, 14, 21 and
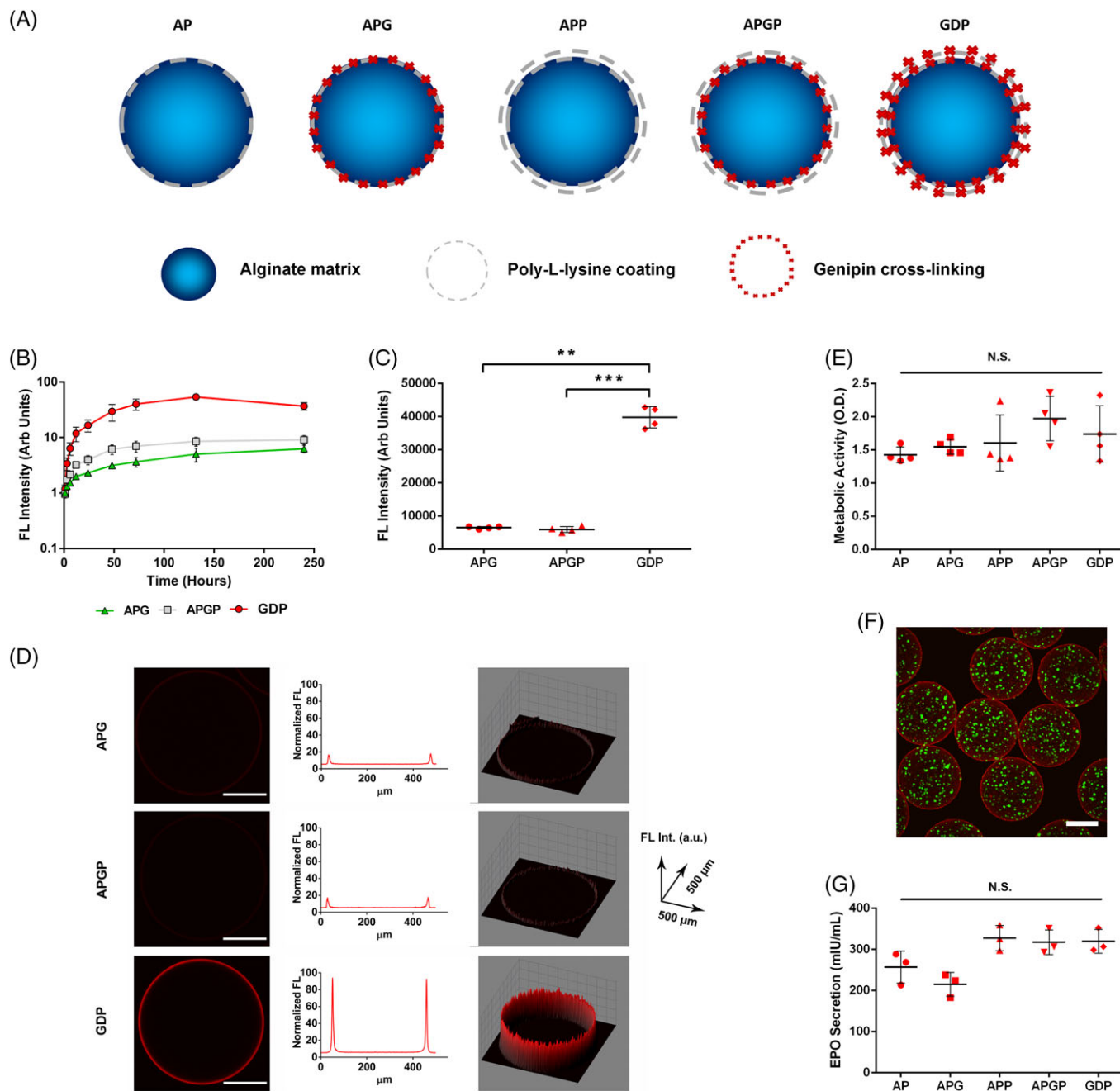
FIGURE 2 GDP microcapsules maximize the fluorescence of genipin while preserving cell viability and function. A, Eschematic depiction showing GDP microcapsules and all the intermediate control groups assayed in the study. B, Reaction kinetics of genipin fluorescence development (Em: 590 nm; Ex: 630 nm) ($n = 4$ samples per group). Error bars, mean $\pm$ SD. C, Fluorescence intensity of microcapsules 96 hours after encapsulation ($n = 4$ samples per group). Error bars, mean $\pm$ SD. **, $P < 0.01$; ***, $P < 0.001$; one-way ANOVA with Tamhane multiple comparison correction. D, Confocal fluorescence analysis of microcapsules. From left to right: representative confocal fluorescence micrographs, profile lines and 3D surface plots of the fluorescence signal distribution and intensity from the equatorial section of microcapsules. Scale bar, 200 μm. E, Metabolic activity of encapsulated D1-MSC-hEPO cells ($n = 4$ samples per group) 96 hours after encapsulation. Error bars, mean $\pm$ SD. N.S. specifies nonsignificant differences against the AP group, $P > 0.05$; one-way ANOVA with Bonferroni multiple comparison correction. Mann-Whitney U test was used with APP group (nonnormal distribution). F, Representative confocal fluorescence image of cells encapsulated in GDP microcapsules and probed with LIVE/DEAD viability kit (Green, living cells; Red, dead cells) 14 days after encapsulation. G, hEPO secretion of immobilized D1-MSC-hEPO cells ($n = 3$ samples per group in duplicate) 96 hours after encapsulation. Error bars, mean $\pm$ SD. N.S. indicates nonsignificant differences against the AP group, $P > 0.05$; one-way ANOVA with Bonferroni multiple comparison correction. FL, fluorescence

35 to validate robustness and long-term stability of this non-invasive visualization strategy (Figure 3D-G). The signal decreased significantly in 50 μL dose by day 21 ($P < 0.05$) but remained relatively stable until day 35. Conversely,

100 and 200 μL doses showed strong signals that did not differ from the initial point throughout the experiment (Figure 3H). Because we injected capsules in PBS, fluorescence signal appears modestly less intense and more diffuse

on the pseudocolor images of day 1. As PBS resorbs, capsules become slightly more localized and fluorescence signal is clearer. Anyhow, differences with respect to day 1 are not significative in any case ($P > 0.05$). As a control for stability of fluorescence, we monitored nonimplanted GDP microcapsules from the same batch in parallel, showing nonsignificant differences in signal throughout the experiment (Figure 4A).

We further analyzed imaging data to validate genipin as a quantitative imaging probe for implanted biomaterials. We first calculated the correlation between administered dose and measured fluorescence signal. A scatter plot of dose vs radiant efficiency and analysis of the linear regression confirmed the linear correlation ($P < 0.001$) and the significance of the slope obtained from the equation ($P < 0.001$). However, the goodness of fit demonstrated that only 66.14%

of the results could be explained by this equation (Figure 4B). Taking into account the high R^2 observed when we used mean values, instead of individual values, for linear regression (Figure 3C), we hypothesized that low precision arisen from either instrument or human error should be behind the poor fitting. In addition, from mean and SD values of the background signal, we estimated the lower limit of detection (LLD) and the lower limit of quantification (LLQ), obtaining doses equivalent to 18.6 and 59.6 µL for each of them, respectively (Figure 4B). This means that the significant signal decay observed for 50 µL dose over time (Figure 3H) should be considered as nonreliable.

Considering the proven stability of the fluorescence signal, we calculated the variability of measurements taken at different time points for each dose as an indicator of the instrument error (repeatability). The lowest dose of 50 µL
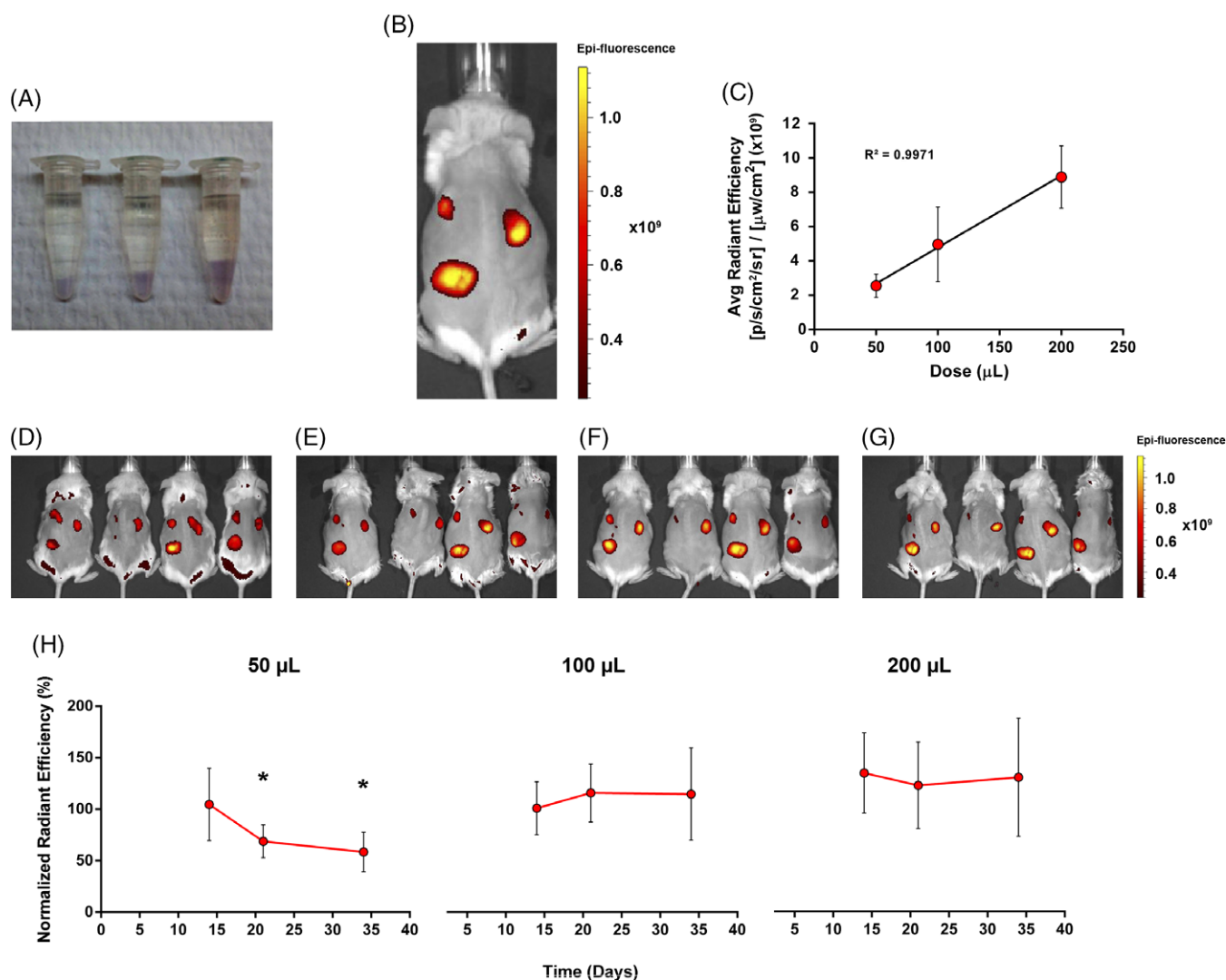

FIGURE 3 GDP microcapsules maintain dose-dependent fluorescence over 35 days in vivo. A, White light image of 50, 100 and 200 µL of GDP microcapsules in 1.5 mL microcentrifuge tubes. B, Representative image of a mouse 21 days after injection of GDP microcapsules. We imaged fluorescence from the microcapsules with 570 nm excitation and 620 nm emission. Scale bar denotes range of photons displayed on a pseudocolor scale with yellow and dark red denoting highest and lowest values, respectively. C, Graph displays dose-dependent response of average radiant efficiency for GDP microcapsules. Error bars, mean ± SD ($n = 4$ per condition). D-G, Panels show representative fluorescence images of mice 1, 14, 21 and 35 days after subcutaneous injection of microcapsules. We used the same pseudocolor scale from panel (B) to display fluorescence. H, Graph shows fluorescence of GDP microcapsules remained relatively constant over 35 days. Data are normalized to day 1 images. Error bars, mean ± SD. *, $P < 0.05$; paired, two-tailed t test, $n = 4$ mice per dose

produced a significantly higher coefficient of variation (CV) (46.5%), whereas 100 and 200 μL doses presented 25.7% and 20.8%, respectively (Figure 4C). These results are comprehensible if we take into account 50 μL dose is below the LLQ. Consequently, the high variability of the lowest dose may be the main determinant of the poor goodness of fit. By isolating this variability, we also determined

the human error in the injections of the microcapsules (ie, dose preparing and administration of microcapsules). Thus, in the present study we estimated a CV of 39.8%, 50.8% and 22.2% for 50, 100 and 200 μL doses respectively (Figure 4D). On the other hand, linear regression analysis of the scatter plot for expected vs measured values confirmed the slope of the equation was equal to 1 ($P < 0.001$) and the
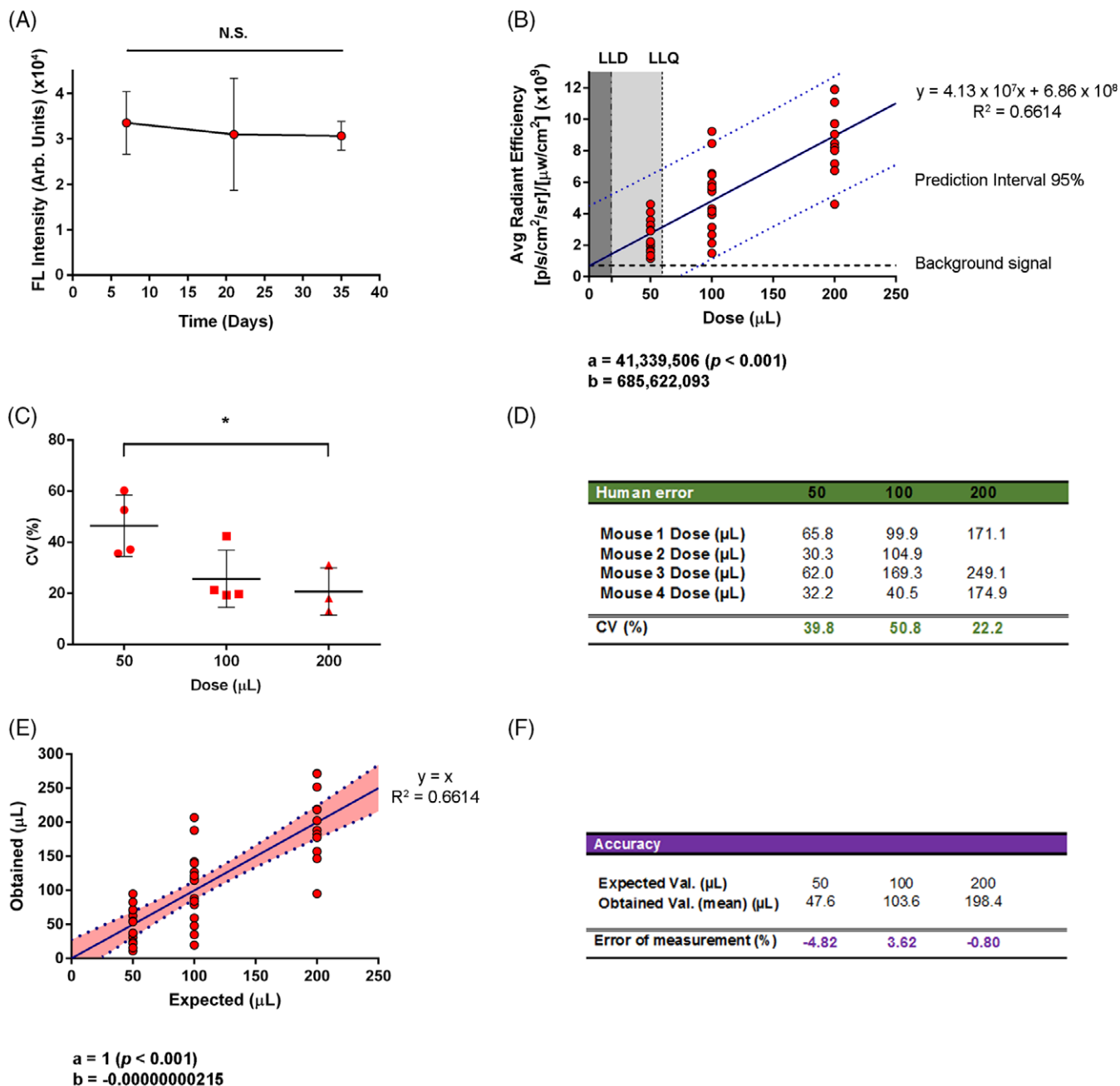

(B) $y = 4.13 \times 10^7 x + 6.86 \times 10^8$
$R^2 = 0.6614$

a = 41,339,506 ($p < 0.001$)
b = 685,622,093

Human error	50	100	200
Mouse 1 Dose (μL)	65.8	99.9	171.1
Mouse 2 Dose (μL)	30.3	104.9	
Mouse 3 Dose (μL)	62.0	169.3	249.1
Mouse 4 Dose (μL)	32.2	40.5	174.9
CV (%)	39.8	50.8	22.2

(E) $y = x$
$R^2 = 0.6614$

Accuracy			
Expected Val. (μL)	50	100	200
Obtained Val. (mean) (μL)	47.6	103.6	198.4
Error of measurement (%)	-4.82	3.62	-0.80

a = 1 ($p < 0.001$)
b = -0.00000000215

FIGURE 4 Analysis of obtained imaging data to validate genipin as a quantitative imaging probe. A, We monitored nonadministered GDP microcapsules in parallel throughout experiment. Error bars, mean $\pm$ SD. N.S., nonsignificant ($P > 0.05$); Paired, two-tailed t test, $n = 5$ independent experiments per time-point. B, Scatter plot of the Dose vs Radiant Efficiency showing the linear regression equation with 95% prediction interval. Each dot in the plot represents an individual measurement for each mouse, time point and dose. The linear correlation was confirmed by ANOVA ($P < 0.001$). The significance of the equation slope was statistically verified by means of the linear regression t test. LLD, lower limit of detection. LLQ, lower limit of quantification. C, Variability of measurements taken at different time points for each dose (repeatability or instrument error). Error bars, mean $\pm$ SD. *, $P < 0.05$; one-way ANOVA with Bonferroni multiple comparison correction, $n = 4$ mice per dose. D, Variability of the injection procedure, reproducibility or human error expressed as the dose calculated for each mouse and the CV of their mean. E, Scatter plot representing the Expected vs Obtained dose values. Each dot in the plot signifies an individual calculated value for each mouse, time point and dose. Colored area within dotted lines, 95% confidence interval. The linear correlation was tested by ANOVA ($P < 0.001$). The significance of the equation slope was statistically proven by a linear regression t test. F, Accuracy of results for each particular dose expressed as error percentage

intercept equal to 0 (Figure 4E). Indeed, the accuracy of the results with all doses was close to the 100% (Figure 4F).

These results reveal that genipin-mediated fluorescence in GDP microcapsules is detectable even at low doses (50 μL is below the usually administered dose) (LLD = 18.6 μL) and reliably quantifiable from 100 μL and higher (LLQ = 59.6 μL). The ability to image GDP fluorescence provides a powerful tool to immediately assess the quality of injection and then monitor stability of microcapsule signal over time with more than acceptable variability of measurements with usually administered doses (>200 μL). Human errors we made and quantified in the present study are common in standard practice in the field of cell microencapsulation but undetectable without the technology described here. Therefore, GDP microcapsules represent a valuable tool to ensure correct administration of the intended dose and improve efficacy and biosafety of cell encapsulation therapies in the clinical routine.

Unlike hydrogels with homogeneous cross-linking throughout their whole volume, GDP microcapsules, as cell-laden alginate microspheres with fluorescence limited to the external membranes (few microns), represent a demanding model for genipin-mediated in vivo imaging. This means that as capsule diameter increases, fluorescence signal related to a particular administered dose diminishes. Therefore, this visualization strategy will work much better when using particle sizes with high surface-area-to-volume ratio. Future studies will also reveal the feasibility of GDP capsule design for other usually used routes of administration, including intraperitoneal, intravitreal or intracranial.

3 | CONCLUSION

In summary, we present a multidisciplinary approach to develop implantable biosystems based on hydrogels with intrinsic fluorescence for in vivo imaging. In particular, we have shown that the use of genipin, an increasingly accepted cross-linker, functions as an excellent quantitative imaging probe to be included in the design of immunoisolation devices. Through this strategy, we have managed to visualize not only the location of the implanted microcapsules, but also to evaluate the actual injected dose, which may improve significantly the efficacy and biosafety of the therapy. As fluorescence imaging systems are gradually implemented in clinical practice, we believe these outcomes will have direct applicability to advance design of multiple hydrogel-based biotechnologies, including drug and cell delivery systems, vaccines or biosensors.

4 | EXPERIMENTAL SECTION

All materials and methods used in this study are thoroughly detailed in the Supporting Information. The University of Michigan IACUC approved all animal procedures.

ORCID

Edorta Santos-Vizcaino https://orcid.org/0000-0001-7064-4563
Ainhoa Gonzalez-Pujana https://orcid.org/0000-0001-6179-8237
Rosa Maria Hernandez https://orcid.org/0000-0002-3947-409X

REFERENCES

[1] J. Liang, X. Dong, C. Wei, D. Kong, T. Liu, F. Lv, *R.S.C. Adv.* **2017**, *7*, 6501.

[2] A. Berdichevski, H. Simaan Yameen, H. Dafni, M. Neeman, D. Seliktar, *Proc. Natl. Acad. Sci. U.S.A.* **2015**, *112*, 5147.

[3] B. P. Barnett, A. Arepally, M. Stuber, D. R. Arifin, D. L. Kraitchman, J. W. Bulte, *Nat. Protoc.* **2011**, *6*, 1142.

[4] A. A. Appel, M. A. Anastasio, J. C. Larson, E. M. Brey, *Biomaterials* **2013**, *34*, 6615.

[5] G. Orive, E. Santos, D. Poncelet, R. M. Hernandez, J. L. Pedraz, L. U. Wahlberg, P. de Vos, D. Emerich, *Trends Pharmacol. Sci.* **2015**, *36*, 537.

[6] A. J. Vegas, O. Veiseh, M. Gurtler, J. R. Millman, F. W. Pagliuca, A. R. Bader, J. C. Doloff, J. Li, M. Chen, K. Olejnik, H. H. Tam, S. Jhunjhunwala, E. Langan, S. Aresta-Dasilva, S. Gandham, J. J. McGarrigle, M. A. Bochenek, J. Hollister-Lock, J. Oberholzer, D. L. Greiner, G. C. Weir, D. A. Melton, R. Langer, D. G. Anderson, *Nat. Med.* **2016**, *22*, 306.

[7] G. Basta, P. Montanucci, G. Luca, C. Boselli, G. Noya, B. Barbaro, M. Qi, K. P. Kinzer, J. Oberholzer, R. Calafiore, *Diabetes Care* **2011**, *34*, 2406.

[8] T. Desai, L. D. Shea, *Nat. Rev. Drug Discov.* **2017**, *16*, 338.

[9] M. Löhr, A. Hoffmeyer, J. Kröger, M. Freund, J. Hain, A. Holle, P. Karle, W. T. Knöfel, S. Liebe, P. Müller, H. Nizze, M. Renner, R. M. Saller, T. Wagner, K. Hauenstein, W. H. Günzburg, B. Salmons, *Lancet* **2001**, *357*, 1591.

[10] J. M. Löhr, S. L. Haas, J. C. Kröger, H. M. Friess, R. Höft, P. E. Goretzki, C. Peschel, M. Schweigert, B. Salmons, W. H. Gunzburg, *Pharmaceutics* **2014**, *6*, 447.

[11] N. G. Kooreman, J. D. Ransohoff, J. C. Wu, *Nat. Mater.* **2014**, *13*, 106.

[12] E. Santos, J. L. Pedraz, R. M. Hernández, G. Orive, *J. Control. Release* **2013**, *170*, 1.

[13] G. A. Paredes-Juarez, P. de Vos, J. W. Bulte, *Expert. Rev. Precis. Med. Drug. Dev.* **2017**, *2*, 57.

[14] R. Catena, E. Santos, G. Orive, R. M. Hernández, J. L. Pedraz, A. Calvo, *J. Control. Release* **2010**, *146*, 93.

[15] E. Santos, L. Larzabal, A. Calvo, G. Orive, J. L. Pedraz, R. M. Hernandez, *Biomaterials* **2012**, *34*, 1442.

[16] A. Goren, N. Dahan, E. Goren, L. Baruch, M. Machluf, *FASEB J.* **2010**, *24*, 22.

[17] A. Paul, G. Chen, A. Khan, V. T. Rao, D. Shum-Tim, S. Prakash, *Cell Transplant.* **2012**, *21*(12), 2735.

[18] H. Chen, W. Ouyang, B. Lawuyi, S. Prakash, *Biomacromolecules* **2006**, *7*(7), 2091.

[19] H. Chen, W. Ouyang, B. Lawuyi, C. Martoni, S. Prakash, *J. Biomed. Mater. Res. A.* **2005**, *75*(4), 917.

[20] A. L. Hillberg, K. Kathirgamanathan, J. B. Lam, L. Y. Law, O. Garkavenko, R. B. Elliott, *J. Biomed. Mater. Res. B Appl. Biomater.* **2012**, *101*, 258.

[21] Y. Zhang, L. Mao, J. Liu, T. Liu, *Mat. Sci. Eng. C.* **2017**, *71*, 17.

[22] X. Dong, Z. Sun, J. Liang, H. Wang, D. Zhu, X. Leng, C. Wang, D. Kong, F. Lv, *Nanomedicine* **2018**, *14*(4), 1087.

[23] G. D. Luker, K. E. Luker, *J. Nucl. Med.* **2008**, *49*(1), 1.

[24] A. Paul, A. Cantor, D. Shum-Tim, S. Prakash, *Mol. Biotechnol.* **2011**, *48*(2), 116.

SUPPORTING INFORMATION

Additional supporting information may be found online in the Supporting Information section at the end of the article.

Appendix S1 Supporting Information

Figure S1 Excitation and emission spectra of genipin cross-linked microcapsules. Emission spectrum, Ex: 514 nm/Em: 550 to 700 nm. Excitation spectrum, Ex: 500-650 nm/Em: 690 nm. Step size, 2 nm. Obtained data are the mean of 4 replicates

Figure S2 D1-MSC-EPO encapsulated in AP microcapsules and subjected to the genipin cross-linking protocols selected in Figure 1B,C. Noncross-linked AP group was used as control. A, Metabolic activity of encapsulated cells after genipin cross-linking. Error bars, mean $\pm$ SD. N.S. nonsignificant differences; one-way ANOVA with Bonferroni multiple comparison correction, $n = 5$ per condition. B, Fluorescence intensity of AP microcapsules after genipin cross-linking. Error bars, mean $\pm$ SD. ***, $P < 0.001$; one-way ANOVA with Bonferroni multiple comparison correction, $n = 5$ samples per condition

Figure S3 Cross-linking reaction kinetics of GDP microcapsules and the intermediate control groups ($n = 4$). Linear least squares fitting method to demonstrate zero order (A) or first order (B) reactions

Figure S4 Diameter size-dependent fluorescence intensity in GDP microcapsules. Error bars, mean $\pm$ SD. **, $P < 0.01$; Unpaired, two-tailed t test, $n = 5$ samples per size

Figure S5 Diameters of GDP microcapsules and intermediate control groups ($n = 15$ capsules per group). Boxes, interquartile range (Q1-Q3); Central point, median; Whiskers, max. and min. Values

Figure S6 A, Zeta potential of PLL chains in solution throughout genipin cross-linking reaction time-course. Error bars, mean $\pm$ SD. *, $P < 0.05$; **, $P < 0.01$; Unpaired, two-tailed t test, $n = 3$ per solution. B, Monitoring of the cross-linking reaction by means of genipin emitted fluorescence. Error bars, mean $\pm$ SD (smaller than markers). ***, $P < 0.001$; Unpaired, two-tailed t test, $n = 3$ per solution

Video S1 3D reconstruction using a stack of confocal images of GDP capsules to show its morphology

Video S2 3D reconstruction displaying fully viable cells (green) within GDP capsules (red). 3D view from a stack of confocal images